Energy xxx (xxxx) xxx-xxx

Contents lists available at ScienceDirect

Energy

journal homepage: www.elsevier.com

Data-driven surrogate assisted evolutionary optimization of hybrid powertrain for improved fuel economy and performance

Debraj Bhattacharjee [a, *], Tamal Ghosh [b], Prabha Bhola [a], Kristian Martinsen [b], Pranab K. Dan [a]

[a] Department: Rajendra Mishra School of Engineering Entrepreneurship (RMSoEE), Institute: Indian Institute of Technology Kharagpur, Kharagpur, 721302, India
[b] Department: Department of Manufacturing and Civil Engineering (IVB), Institute: Norwegian University of Science and Technology, Teknologivegen 22, 2815, Gjøvik, Norway

ARTICLE INFO

Article history:
Received 24 March 2019
Received in revised form 24 May 2019
Accepted 17 June 2019
Available online xxx

Keywords:
Component sizing
Hybrid electric vehicle
Energy efficiency
Many-objective optimization
NSGA III
Surrogate assisted evolutionary optimization

ABSTRACT

This article presents an optimized series-parallel hybrid powertrain transformed from a conventional vehicle using an analytical approach without changing the original chassis. The proposed approach is based on a many-objective hybrid powertrain model, which aims to optimize the vehicle weight, fuel consumptions, emissions, and performances. Three different Surrogate Assisted Evolutionary Algorithms (SAEAs) are introduced based on the improved Non-dominated Sorting Genetic Algorithm (NSGA III), Multi-Objective Evolutionary Algorithm Based on Decomposition (MOEA/D) and Multi-Objective Genetic Algorithm (MOGA) for optimization of powertrain components. Initially, the powertrain optimization is performed for Urban Dynamometer Driving Schedule (UDDS) driving cycle with 20% road grade. Thereafter, all the obtained Pareto solutions are combined, screened, and 78 best feasible design points are considered depending on the constraints imposed. Subsequently, 15 design points are randomly selected for validation in Federal Test Procedure (FTP) driving cycle without road grade. It is observed that NSGA III reduces the vehicle weight and fuel consumptions by 4.39% and 46.47% respectively. The powertrain energy efficiency is improved by 57.49%, and the engine is downsized by 40%. The contribution of this article is twofold. First, the many-objective simulation model for hybrid powertrain is developed. Second, SAEAs are implemented as optimization techniques for optimal component sizing and promising results are obtained.

Abbreviations

IC	Internal Combustion
FTP	Federal Test Procedure
DT	Decision Tree
FC	Fuel Consumption
CO_2	Carbon-di-oxide
CO	Carbon Monoxide
HC	Hydrocarbon
DOE	Design of Experiment
DC	Direct Current
SOC	State of Charge
DE	Differential Evolution
GP	Gaussian Process
GA	Genetic Algorithm
GP	Genetic Programming
EA	Evolutionary Algorithm
FFD	Full Factorial Design
OE_D	Drivetrain efficiency
MSE	Mean Square Error
MOGA	Multi-Objective Genetic Algorithm
MOEA/D	Multi-Objective Evolutionary Algorithm Based On Decomposition
NSGA	Non-dominated Sorting Genetic Algorithm
HWFET	Highway Fuel Economy Test
SAEA	Surrogate Assisted Evolutionary Algorithm
WLTP	Worldwide Harmonised Light Vehicle Test Procedure
PSO	Particle Swarm Optimization
NOX	Nitrogen Oxide Component
UDDS	Urban Dynamometer Driving Schedule
PMS	Power management strategy
HEV	Hybrid Electric Vehicle
SVM	Support Vector Machine
ANN	Artificial Neural Network
BNN	Bayesian Neural Network
LHS	Latin Hypercube Sampling
OAD	Orthogonal Array Design
NREL	National Renewable Energy Laboratory NREL
MOPs	Multi-objective Optimization Problems

Symbols

m_{veh}	Vehicle mass (kg)
P_{eng}	Engine power (kW)
P_{maxeng}	Engine maximum power (kW)
ω_{eng}	Engine angular velocity(rps)
τ_{eng}	Engine torque (Nm)
P_{maxmot}	Maximum Motor power (kW)

* Corresponding author.
Email addresses: debraj1@iitkgp.ac.in (D. Bhattacharjee); tamal.ghosh@ntnu.no (T. Ghosh); prabha@see.iitkgp.ac.in (P. Bhola); kristian.martinsen@ntnu.no (K. Martinsen); pkdan@see.iitkgp.ac.in (P.K. Dan)

https://doi.org/10.1016/j.energy.2019.06.115
0360-5442/

Table 1
Initial vehicle parameters.

Parameters	Conventional Vehicle	Toyota Prius
Vehicle mass (m_{veh})	1195 Kg	1404 Kg
Engine maximum power (P_{maxeng})	70 kW	43 kW
Motor maximum power (P_{maxmot})	–	31 kw
Generator max power (P_{maxgen})	–	15 kW
Aerodynamic drag coefficient (C_D)	0.19	0.30
Front area (A_f)	2.038 m^2	1.7460 m^2
Vehicle CG height (h_{cg})	0.4 m	0.569 m
Vehicle wheel radius (r_w)	0.2820 m	0.2870 m
Transmission gear ratio/ Power-split	13.195; 7.3486; 4.9126; 3.4916; 2.5984	3.93

$P_{mot,loss}$ Motor power loss (kW)
μ_{mot} Motor efficiency
P_{mot} Motor Power (kW)
ω_{mot} Motor angular velocity (rps)
$P_{mot,in}$ Motor power input (kW)
$P_{mot,o}$ Motor power output (kW)
$S_{eng,\omega}$ Engine speed scale
$S_{eng,p}$ Engine power scale
$S_{eng,\tau}$ Engine torque scale
$S_{eng,m}$ Engine mass scale
$S_{mot,p}$ Motor power scale
$S_{mot,\omega}$ Motor angular velocity scale
$S_{mot,\tau}$ Motor torque scale
J_{engine} Engine inertia(kg-m^2)
τ_{mot} Motor torque (Nm)
ω_{mot} Motor speed (rps)
CO_{eng} Carbon monoxide emission (gm/km)
HC_{eng} Hydrocarbon emission (gm/km)
NOX_{eng} Nitrox emission (gm/km)
P_{gen} Generator power (kW)
ω_{gen} Generator angular velocity (rps)
τ_{gen} Generator torque (Nm)
$P_{gen,out}$ Generator useful power (kW)
μ_{gen} Generator efficiency
m_{gen} Generator mass (Kg)
$S_{gen,m}$ Generator mass scale
FC Vehicle fuel consumption per 100 km (lit/100 km)
f_{max} Vehicle maximum acceleration (m/s^2)
N_r Teeth number of Ring gear
τ_w Wheel torque (Nm)
η_0 Final drive efficiency
$i0$ Final drive ratio
η_g Power-split efficiency
i_g Transmission ratio
τ_b Mechanical brake torque (Nm)
δ Mass correction factor
r_w Tire radius (m)
h_{cg} Vehicle CG height (m)
g Gravitational acceleration
T Temperature (^oC)
ω_{out} Output angular velocity to the tire (rps)
τ_{out} Output torque to the tire (Nm)
k Ratio between ring teeth number and sun teeth number
fr Rolling coefficient
θ Road grade angle
C_D Aerodynamic drag coefficient
A_f Front area of vehicle(m^2)
ρ_{air} Air density (Kg/m^3)
v_{veh} Vehicle velocity(Km/hr)
P_{bat} Battery power(kW)
I Battery current (amp)
V_{max} Vehicle maximum velocity (Km/hr)
C_{max} Maximum battery charge (Ah)
C_{used} Used charge (Ah)
N_{bat} Number battery module
m_{bat} Battery mass (Kg)
$S_{gen,\tau}$ Generator Torque scale
$S_{gen,\omega}$ Generator angular velocity scale
$S_{gen,p}$ Generator power scale
$P_{max,gen}$ Generator maximum power(kW)
f_{eng} Fuel consumption (gm)
$\%accelearation\ dev$ Percentage acceleration deviation
$Diff\_SOC$ SOC difference
N_s Teeth number of Sun gear

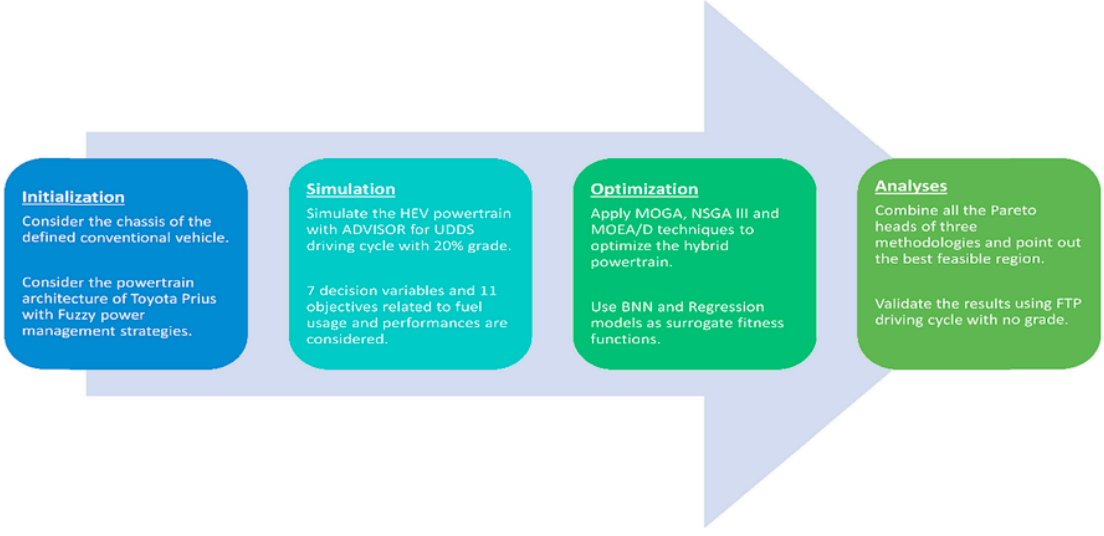

Fig. 1. Proposed work-flow for multi-objective HEV powertrain optimization.

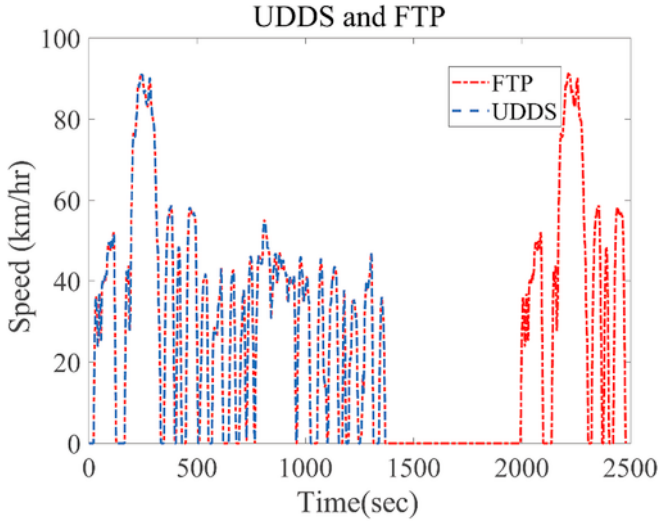

Fig. 2. FTP and UDDS driving cycles.

1. Introduction

The HEV is considered as a significant add-on in the cluster of the alternative vehicles, which is an energy efficient and cost-effective solution for the automotive industry [1]. Holistic efficiency of the HEV depends on its powertrain performance, which further depends on its electro-mechanical components. These components are to be designed more optimally to tune the overall performance of the powertrain. Accurate sizing of these components would also be essential in order to optimize the hybrid powertrain. Recently the component-sizing problem of HEV becomes popular in automotive research, which is further divided into two broader categories (1) selection of influential powertrain components while converting a conventional powertrain to a hybrid powertrain and (2) downsizing the powertrain components to obtain optimal fuel consumptions, emissions, and vehicle performances. According to the automotive literature, the solution methodologies for the component sizing problems are classified as, sequential, iterative, bi-level, and simultaneous optimization problems [2]. The sequential methods could be found in the studies recently proposed in Refs. [3,4]. In case of sequential method, the control laws are defined based on the component sizes for the power management system. On the other hand, iterative methods optimize

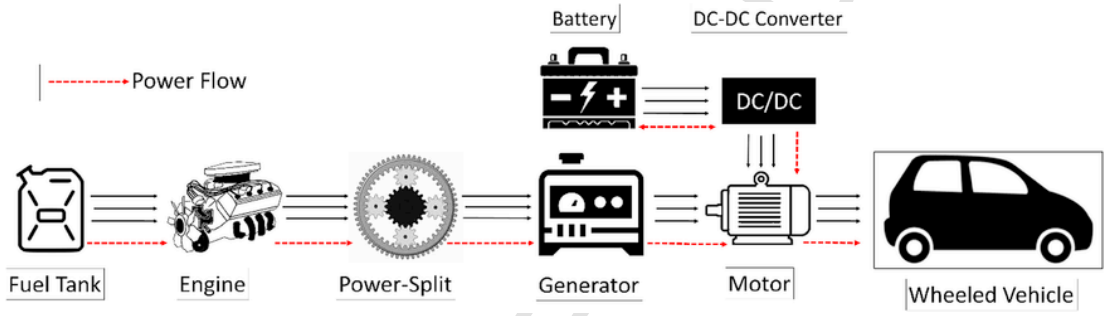

Fig. 3. Power-Split HEV architecture.

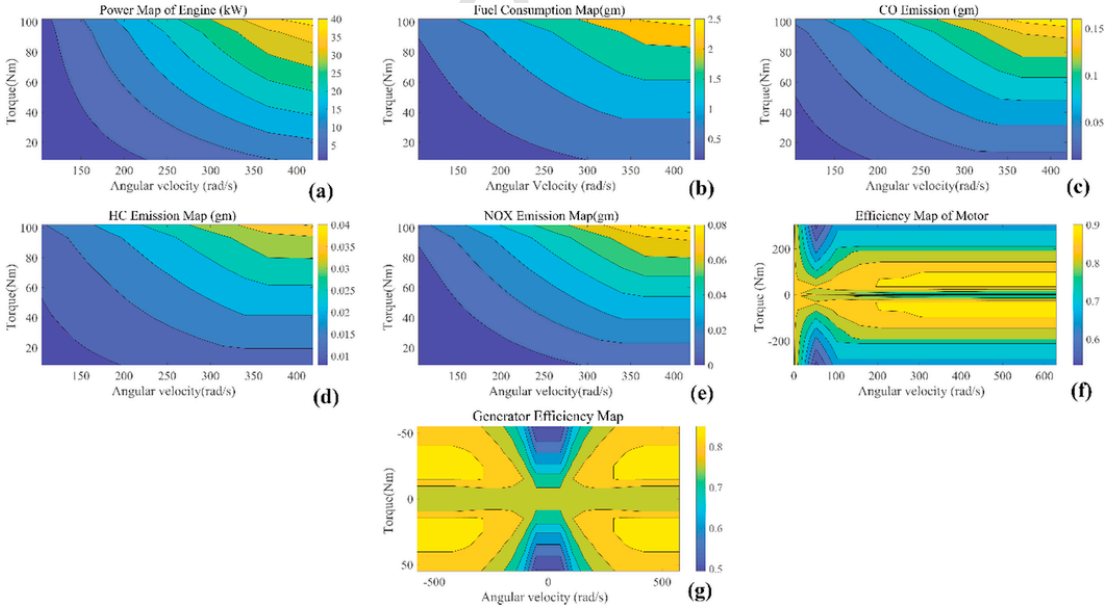

Fig. 4. Powertrain components descriptions using contour plots: (a) Power map of engine (b) Fuel consumption map (c) CO emission map (d) HC emission map (e) NOX emission map (f) Motor efficiency map (g) Generator efficiency map.

Table 2
Fuzzy rule based PMS.

SOC	Grade	Velocity	Torque demand	Engine	Motor	Generator
Less than lower threshold	Greater than lower threshold	Higher than higher threshold	Less than lower threshold and greater than higher threshold	ON	GEN	ON
Greater than lower threshold	Less than higher threshold	Greater than higher threshold	Greater than lower threshold and lower than higher threshold	ON but disengaged from powertrain	ON	ON
Greater than lower threshold and lower than higher threshold	Less than higher threshold	Less than higher threshold	Any Value	OFF	ON	OFF
Greater than higher threshold	Lower than lower threshold	Less than higher threshold	Less than lower threshold	OFF	ON	ON
Greater than higher threshold	Greater than higher threshold	Greater than higher threshold	Greater than higher threshold	ON	ON	OFF

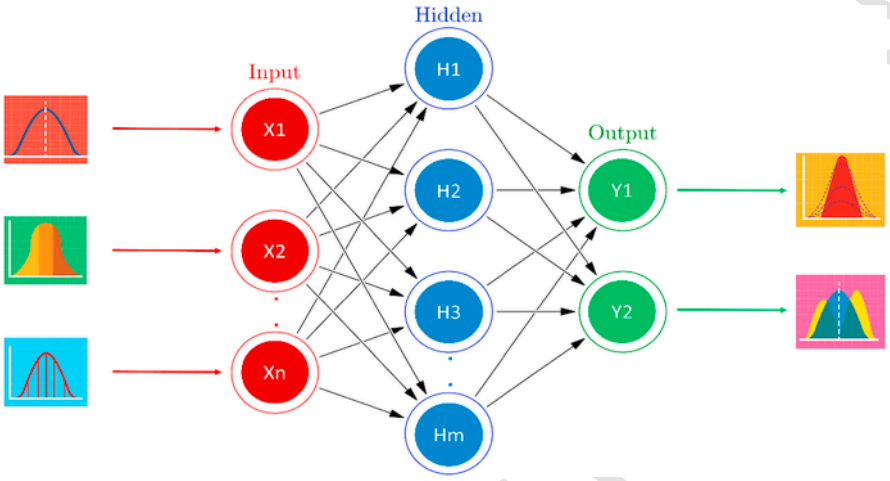

Fig. 5. BNN schematic diagram.

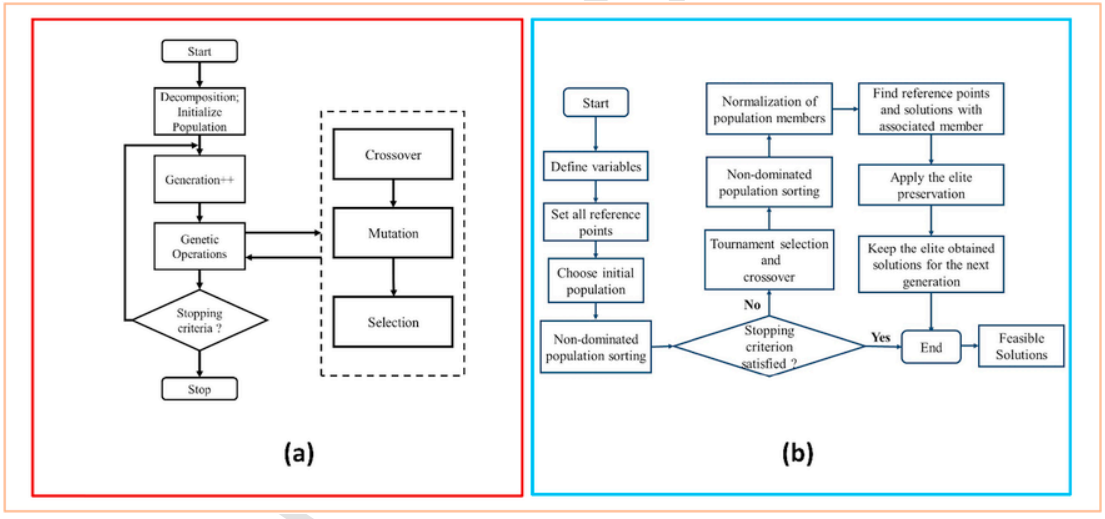

Fig. 6. (a) MOEA/D flowchart (b) NSGA III flowchart.

the component sizes and control laws until the component sizes converge without compromising the desired performance [5]. In simultaneous method, the component size and control laws are selected simultaneously for every cycle of computation [6]. The Bi-level method utilizes two nested optimization loops in order to achieve the global best objective values [7]. Component sizing is a multi-objective optimization problem, which could enhance the system efficiency by minimizing the fuel usage of the engine and the loss of the system in a hybrid powertrain. Based on the powertrain architecture, the powertrain could be classified as series, parallel, and series-parallel architectures. Driving cycles might have an effect on the powertrain component sizing [8]. Therefore, some of the studies portray the combined form of the different driving cycles, which minimizes the variations in the fuel economy of a particular HEV powertrain architecture [9,10]. However, a holistic optimization model is not yet found in automotive literature. In a recent study [11], authors applied

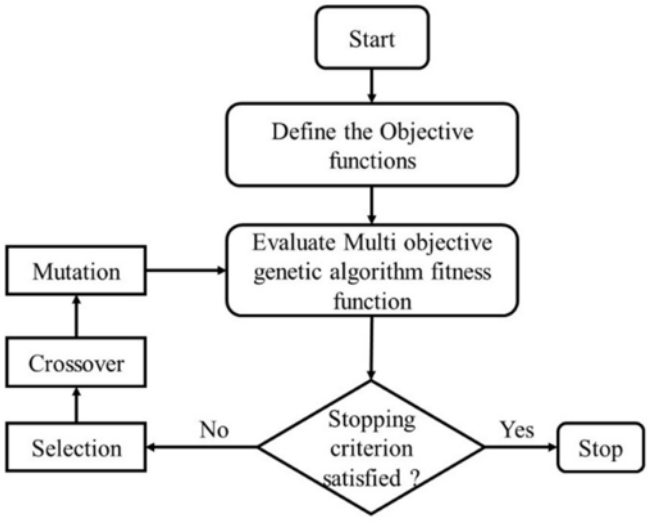

Fig. 7. Algorithm for MOGA

Chaos-enhanced Accelerated PSO to find the feasible solution points with an effective Pareto analysis, which shows that equal weights consideration for the bi-objective problem could obtain improved solution. In Ref. [12] the objectives considered, were the minimization of two different types of fuel consumptions. A plugin-type HEV with power-split is considered for the design space exploration, and PSO is used as main optimization algorithm. The gear ratios and the traction components are optimized based on the different driving modes. Design space exploration recommends a set of Pareto solution points instead of single optimal design point since the problem is multi-objective type [13,14]. In Ref. [15], the fuel consumption and carbon emission have been considered as the primary objectives for converting a conventional vehicle to HEV. The conversion shows that the CO_2 emission could be minimized by 23% and operational cost by 26% through hybridization of a conventional vehicle. Ref. [16] depicts the best transmission configuration in a plug-in HEV by minimizing the fossil fuel consumption and total energy consumption. The number of gears and gear ratios are considered as variables. The result shows an improvement in the fuel economy by 7.79%, 9.74% and 4.41% for three driving cycle namely FTP, UDDS, and WLTP respectively. The authors of ref. [17] successfully downsized the main traction motor in a plugin hybrid vehicle from 120 KW to 30 KW for the harmonised vehicle driving cycle. Not only the component sizing,

Table 3
Regression models with P Values and R^2 Values.

Objective Models	*P value* for Decision Variables							R^2
	P_{maxeng}	P_{maxmot}	P_{maxgen}	i_0	N_{bat}	N_r	N_s	
m_{veh}	0.000	0.000	0.000	–	0.000	–	–	98%
FC	0.004	0.778	0.432	0.000	0.004	0.003	0.234	80.28%
%accelearation dev	0.000	0.426	0.480	0.000	0.200	0.009	0.000	87.18%
HC	0.033	0.792	0.478	0.000	0.004	0.001	0.022	78.69%
CO	0.019	0.790	0.488	0.000	0.004	0.001	0.031	79.37%
NOX	0.009	0.831	0.405	0.000	0.005	0.002	0.153	79.21%
Failed to travel	0.000	0.132	0.153	0.000	0.038	0.017	0.000	90.63%
Speed error	0.002	0.076	0.285	0.000	0.004	0.148	0.003	79.86%
diff _ SOC	0.004	0.367	0.052	0.006	0.223	0.557	0.002	68.45%
V_max	0.544	0.677	0.099	0.000	0.003	0.116	0.167	82.14%
f _max	0.38	0.000	0.229	0.000	0.183	0.205	0.785	86.98%

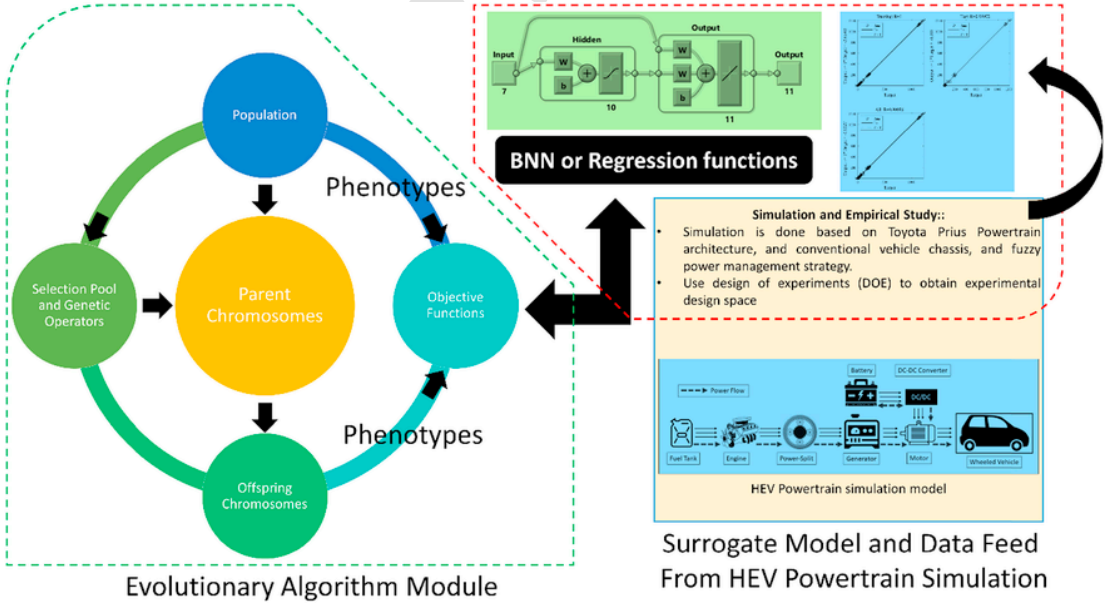

Fig. 8. SAEA framework for HEV Powertrain.

Table 4
HEV powertrain Parameters and their levels for L^{27} Orthogonal Array.

Factors	Level 1	Level 2	Level 3
P_{maxeng}	30	40	50
N_{bat}	20	30	40
P_{maxmot}	30	40	50
P_{maxgen}	15	20	25
N_r	50	64	78
N_s	18	24	30
i_0	2.5	3.0	3.93

but also the topology selection could be found in other studies [18], which improves fuel economy by 14.4% and 44.9% in 2 different driving cycles. The results show an 1.5% gross vehicle weight reduction, 11% traction motor efficiency improvement, and 21% fuel economy improvement. Product cost based optimization for a series plug-in HEV could be found in the ref. [19]. Three different methods are applied to obtain the solution points, namely Second Order Cone Program, Linear Program, and Energy Based methods for a plugin HEV. Another study presents a specialized model for determining the powertrain component sizing, weight and product cost estimation [20]. The authors have used this model for further component selection for powertrain of HEV. The study portrayed by Ref. [21] could estimate the thermal and dynamic characteristics of a traction motor operating in overcurrent region for HEV, where traction motor was downsized and 6.97% improvement in energy consumption and 5.7% efficiency in fuel consumption was achieved. The authors of ref. [22] used the pontrayagin's minimum principle for sizing of battery pack. The transmission ratios are searched for achieving the minimum fuel consumption in Ref. [23]. A component sizing operation on a Toyota Prius could be obtained from the ref. [24], which shows an improvement in fuel economy by 6.56% in FTP driving cycle and 3.15% in the HWFET with respect to original design. In Ref. [25] ride comfort, power performance and energy consumption are considered as objectives for the component resizing of a HEV powertrain.

In this article, an effort is made to formulate a novel many-objective HEV powertrain model that simultaneously optimizes eleven objectives for a series parallel HEV. Such type of complex many-objective optimization problem for HEV powertrain is not yet attempted in past. The parameters for the HEV powertrain are considered from a real vehicle. The initial modeling data are produced through computer simulation for UDDS driving cycle with 20% grade. The formulated many-objective problem has been solved with three latest SAEAs, namely NSGA III, MOEA/D and MOGA, which utilize the deep learning based BNN and regression models. The fuzzy power management strategy is considered to control the powertrain. The objectives are based on minimization of vehicle weight, fuel consumption, emission of the hydrocarbon and carbon monoxide and nitrox, percentage acceleration deviation, failed to travel distance, speed deviation, and maximization of vehicle speed and acceleration. Total 78 Pareto solutions are selected from the combined list of all solutions and 15 design points are picked and validated in FTP driving cycle without any grade. The analyses conclude that the conversion of the conventional vehicle to an optimized HEV enhances the fuel efficiencies and performances. The rest of this study proceeds in following order, Section #2 introduces the HEV powertrain and its component modeling. Section #3 demonstrates the proposed SAEAs. Section #4 presents the results and analyses and Section #5 concludes this research.

2. Powertrain of HEV

This article deals with two problems (1) conversion of a conventional vehicle to a HEV and (2) optimization of powertrain using component sizing. Table 1 portrays the description of a conventional vehicle based on Toyota Prius powertrain model. The workflow of this research is depicted in the Fig. 1.

The initial data are produced for powertrain using simulation study based on a real vehicle for UDDS driving cycle with 20% grade. At the end, the validation study is conducted using FTP driving cycle without grade. The two driving cycles are portrayed in the Fig. 2. Any driving cycle could directly affect the fuel consumption for the vehicle. Therefore, the testing of the final design points needs to be carried out in another different driving cycle for validation. The testing of the initial vehicle model was conducted on the UDDS driving cycle (blue line in Fig. 2). Hence, the improvement in the final design points is verified in the FTP driving cycle (red line in Fig. 2). This way, the superiority of the design points is validated.

2.1. Powertrain modeling

The series parallel HEV architecture is depicted in Fig. 3. Whereas, Fig. 4 presents the detailed characteristics of the powertrain components of Toyota Prius system, which are engine power map, engine fuel map, emission maps, Motor efficiency map, CO, HC, NOX emission maps, and generator efficiency map. The depicted powertrain has been considered for optimization. The mathematical models of the powertrain components are described next.

2.1.1. IC engine modeling

The IC engine model could be demonstrated using mathematical expression, which is further decomposed into maximum power model, fuel consumption model, CO_2 emission model, HC emission model and NOX emission model. The power of the engine (KW) could be expressed using Eq. (1).

$$P_{eng} = \frac{\omega_{eng} \times \tau_{eng}}{1000} \tag{1}$$

For component sizing, the scale factors are introduced in this work, which could change other parameters with changes in engine maximum power. Eq. (2) depicts the engine maximum power as a function of engine torque, speed, and scale factor for the maximum power of the engine.

$$P_{maxeng} = \frac{Max\left[\omega_{eng} \times \tau_{eng}\right]}{1000} \times S_{eng,p} \tag{2}$$

$$S_{eng,p} = S_{eng,\omega} \times S_{eng,\tau} \tag{3}$$

The mass of the engine m_{eng} could be defined using Eq. (4). The J_{engine} (Eq. (5)) is presented as the function of engine power scale factor.

$$m_{eng} = f_m\left(P_{maxeng}\right) \tag{4}$$

$$J_{engine} = f_j\left(S_{eng,p}\right) \tag{5}$$

The f_{eng} (gram/KW) is portrayed in Eq. (6), which is the function of speed and torque at a particular moment t (Eq. (7)).

Table 5
HEV powertrain Parameters in Taguchi's L^{27} table.

Exp. #	P_{maxeng}	N_{bat}	P_{maxmot}	P_{maxgen}	N_r	N_s	i_0	m_{veh}	FC	% accelearation dev	HC	CO	NOX	E_L	Speed dev	diff_SOC	V_max	f_max
1	50	40	50	25	78	30	3.93	1217	20.3	5.419	1.362	2.036	0.878	0	0.4054	0.2387	162.1	4.7
2	50	40	50	25	64	24	3	1217	28.3	7.2091	1.51	2.227	0.9	4.4	0.4733	0.2422	203.9	4.6
3	50	40	50	25	50	18	2.5	1217	37.1	11.3428	2.192	3.178	1.212	7	0.5720	0.2486	203.6	3.8
4	50	30	40	20	78	30	3.93	1176	25.6	3.6567	1.244	1.866	0.797	2.2	0.3172	0.2369	162.1	4.7
5	50	30	40	20	64	24	3	1176	32	9.2237	1.801	2.631	1.036	5.7	0.5559	0.2475	196.1	3.8
6	50	30	40	20	50	18	2.5	1176	44	12.9186	2.722	3.913	1.457	7.9	0.6443	0.2489	196.7	3.1
7	50	20	30	15	78	30	3.93	1134	26.9	5.4585	1.405	2.072	0.854	3.4	0.5471	0.2474	162.8	3.1
8	50	20	30	15	64	24	3	1134	33.6	10.144	2.013	2.898	1.107	6.2	0.7048	0.2483	194.9	2.6
9	50	20	30	15	50	18	2.5	1134	77.7	16.527	5.871	8.176	2.729	10.1	0.7743	0.2499	193.9	2.3
10	40	40	40	15	78	24	2.5	1148	55.7	15.8001	3.552	5.142	1.862	9.7	0.6479	0.2511	218.8	3.2
11	40	40	40	15	64	18	3.93	1148	24.9	8.6733	1.308	1.958	0.795	5.3	0.4901	0.2459	161.8	4.7
12	40	40	40	15	50	30	3	1148	35.4	10.1384	1.591	2.453	1.094	6.2	0.5449	0.2482	213.4	3.8
13	40	30	30	25	78	24	2.5	1140	75.2	16.8946	5.056	7.207	2.542	10.4	0.7341	0.2501	206.9	2.5
14	40	30	30	25	64	18	3.93	1140	29.1	11.0036	1.654	2.443	0.952	6.7	0.5676	0.2487	162.4	4
15	40	30	30	25	50	30	3	1140	25.1	4.4907	1.058	1.651	0.763	2.8	0.3952	0.2382	162.6	3.9
16	40	20	50	20	78	24	2.5	1155	103.5	17.7114	7.347	10.35	3.544	10.9	0.7546	0.2501	194.9	3.5
17	40	20	50	20	64	18	3.93	1155	27.7	10.6817	1.618	2.365	0.911	6.6	0.5829	0.2494	162.6	4.7
18	40	20	50	20	50	30	3	1155	25.1	4.9759	1.099	1.704	0.772	3.1	0.4543	0.2419	162.9	4.7
19	30	40	30	20	78	18	3	1112	51.1	16.8463	3.52	5.181	1.792	10.3	0.6735	0.2501	209.6	3
20	30	40	30	20	64	30	2.5	1112	58	16.0224	2.9	4.419	1.842	9.8	0.7049	0.25	203.3	2.5
21	30	40	30	20	50	24	3.93	1112	26.5	10.1842	1.16	1.819	0.818	6.2	0.5427	0.2475	162.8	3.9
22	30	30	50	15	78	18	3	1128	56.1	17.1482	3.908	5.603	1.917	10.5	0.6735	0.2512	194.7	4.7
23	30	30	50	15	64	30	2.5	1128	64.2	16.4661	3.307	5.028	2.062	10.1	0.6779	0.2495	194	3.9
24	30	30	50	15	50	24	3.93	1128	24.7	9.6562	1.102	1.722	0.768	5.9	0.5362	0.2481	162.8	4.7
25	30	20	40	25	78	18	3	1119	101.6	18.3215	7.687	10.749	3.515	11.2	0.7553	0.2506	178.9	3.6
26	30	20	40	25	64	30	2.5	1119	99.1	17.6469	5.401	8.101	3.228	10.8	0.7604	0.2509	180.9	3
27	30	20	40	25	50	24	3.93	1119	28.8	11.5256	1.364	2.104	0.91	7.1	0.6326	0.2481	163.2	4.7

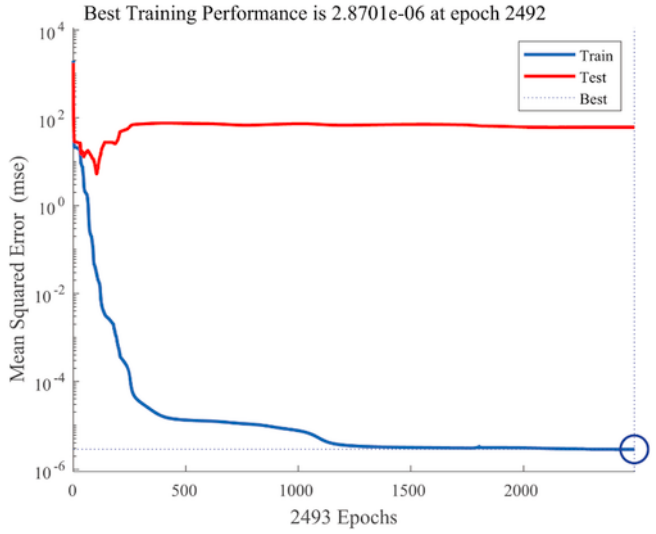

Fig. 9. Performance Curve for the BNN surrogate.

$$f_{eng} = \frac{f_{eng}}{P_{eng} \times 3600} \tag{6}$$

$$f_{eng} = f\left(\omega_{eng},\ \tau_{eng}\right) \tag{7}$$

The emission of CO, HC, and NOX could be depicted using Eq. (8)-(10).

$$CO_{eng} = CO\left(\omega_{eng},\ \tau_{eng}\right) \tag{8}$$

$$HC_{eng} = HC\left(\omega_{eng},\ \tau_{eng}\right) \tag{9}$$

$$NOX_{eng} = NOX\left(\omega_{eng},\ \tau_{eng}\right) \tag{10}$$

2.1.2. Electric motor modeling

The mathematical expressions of the electric motor could be exhibited using Eq. (11) – (16).

$$P_{mot} = \tau_{mot} \times \omega_{mot} \tag{11}$$

$$P_{mot,loss} = \left[\left(\frac{1}{\mu_{mot}\left(\omega_{mot}, \tau_{mot}\right)}\right) - 1\right] \times P_{mot} \tag{12}$$

Here the efficiency of the motor is the function of the angular velocity and torque of the motor. The $P_{mot,\ max}$ is function of $P_{mot,\ in}$ and $P_{mot,o}$,

$$P_{mot,\ in} = P_{mot,\ o} + P_{mot,\ loss} \tag{13}$$

The maximum value of the motor power is related to other motor parameters with the scale factor.

$$S_{mot,p} = S_{mot,v} \times S_{mot,\tau} \tag{14}$$

$$P_{mot,max} = \max\left(P_{mot}\right) \tag{15}$$

The mass of the motor is also related to maximum motor power with a mass scale factor. The relation could be expressed as,

$$m_{mot} = S_{mot,m} \times P_{maxmot} \tag{16}$$

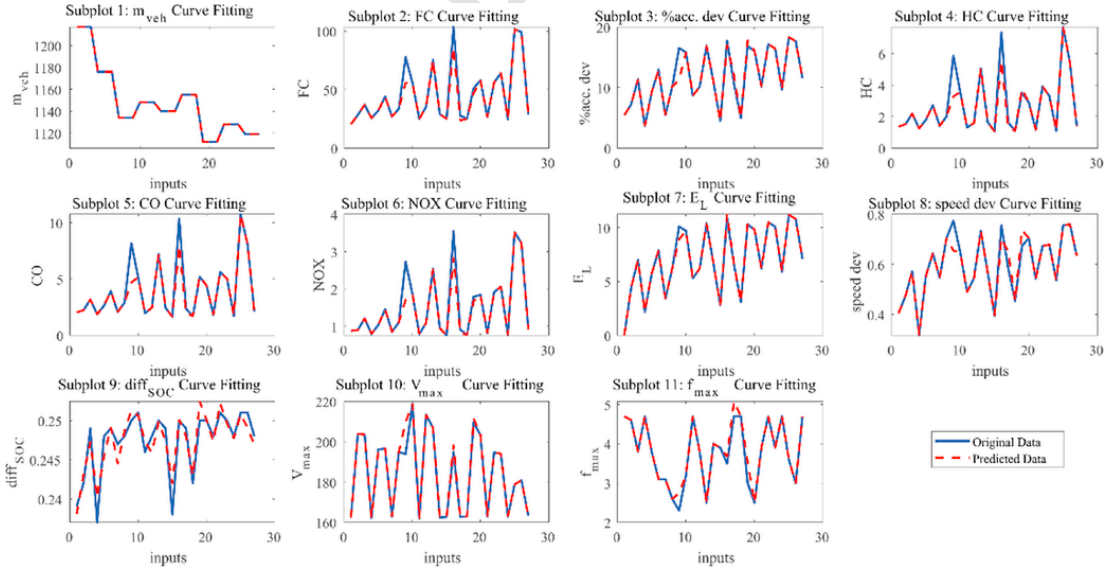

Fig. 10. Original and predictive data plotted for eleven responses of HEV powertrain using BNN.

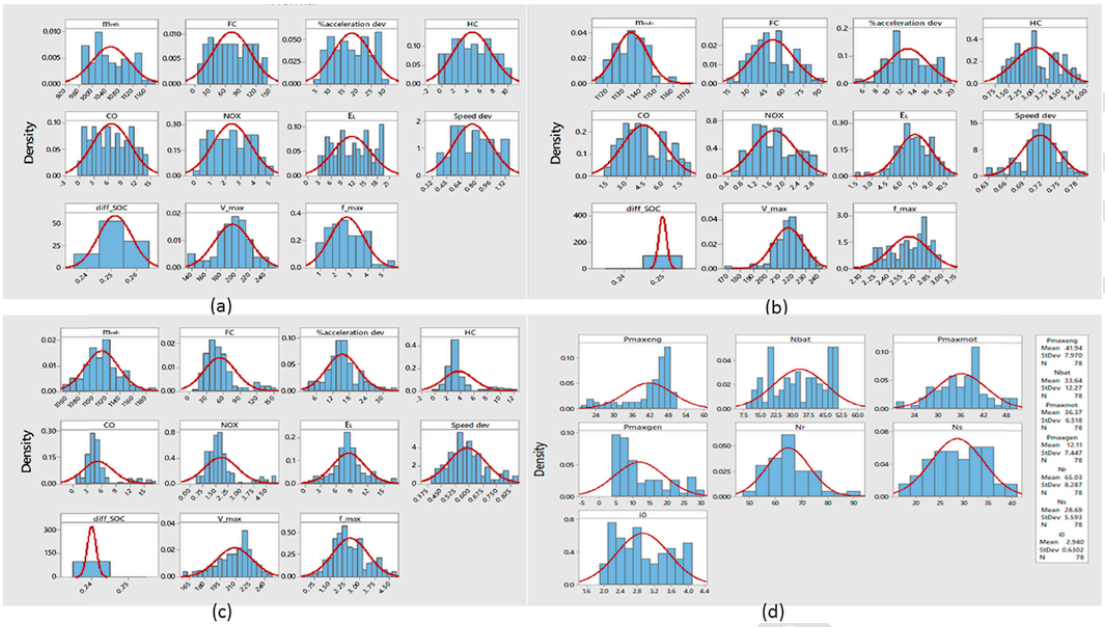

Fig. 11. Probability distributions for (a) MOGA Results, (b) NSGA III Results and (c) MOEA/D Results, and (d) 78 design point (parametric combinations).

Table 6
Objective mean and standard deviations (SD).

objectives	MOGA		NSGA III		MOEA/D	
	Mean	SD	Mean	SD	Mean	SD
m_{veh}	1056.00	56.27	1135.00	9.86	1113.00	25.46
FC	72.74	38.07	50.24	17.31	53.69	28.49
% acceleration dev	17.77	6.98	12.76	3.16	15.25	5.78
HC	4.67	2.89	3.07	1.22	3.57	2.32
CO	6.73	4.04	4.44	1.73	5.09	3.19
NOX	2.41	1.30	1.69	0.60	1.83	0.98
E_L	11.32	4.97	7.29	1.69	8.27	3.04
Speed dev	0.7596	0.2096	0.7175	0.0321	0.5875	0.1023
Diff_SOC	0.2515	0.0067	0.2499	0.0009	0.2402	0.0012
V_{max}	196.30	24.96	216.40	11.83	209.90	18.10
f_{max}	2.689	1.071	2.629	0.216	2.571	0.843

2.1.3. Generator modeling

The mathematical model for generator could be expressed using Eq. (17) and Eq. (18)

$$P_{gen} = \tau_{gen} \times \omega_{gen} \tag{17}$$

$$P_{gen} = \frac{P_{gen,out}}{\mu_{gen}} \tag{18}$$

The mass of the vehicle and power is related with other factors with scale factors. The other relations are provided in the Eq. (19) - (20).

$$m_{gen} = S_{gen,m} \times P_{maxgen} \tag{19}$$

$$S_{gen,p} = S_{gen,v} \times S_{gen,\tau} \tag{20}$$

2.1.4. Battery modeling

The battery could be modelled using Eq. (21)-(23). The considered battery model is based on a lithium ion battery. The single battery module charge capacity is 6Ah. The mass of the battery module m_{bat} is the function of number of battery module N_{bat}.

$$m_{bat} = f_m\left(N_{bat}\right) \tag{21}$$

The SOC has been defined as the ratio of remaining charge and maximum charge C_{max}. The model uses the charge used (C_{used}) with current (I), and temperature (T).

$$SOC = \frac{C_{max} - C_{used}}{C_{max}} \tag{22}$$

$$C_{used} = C(I, T) \tag{23}$$

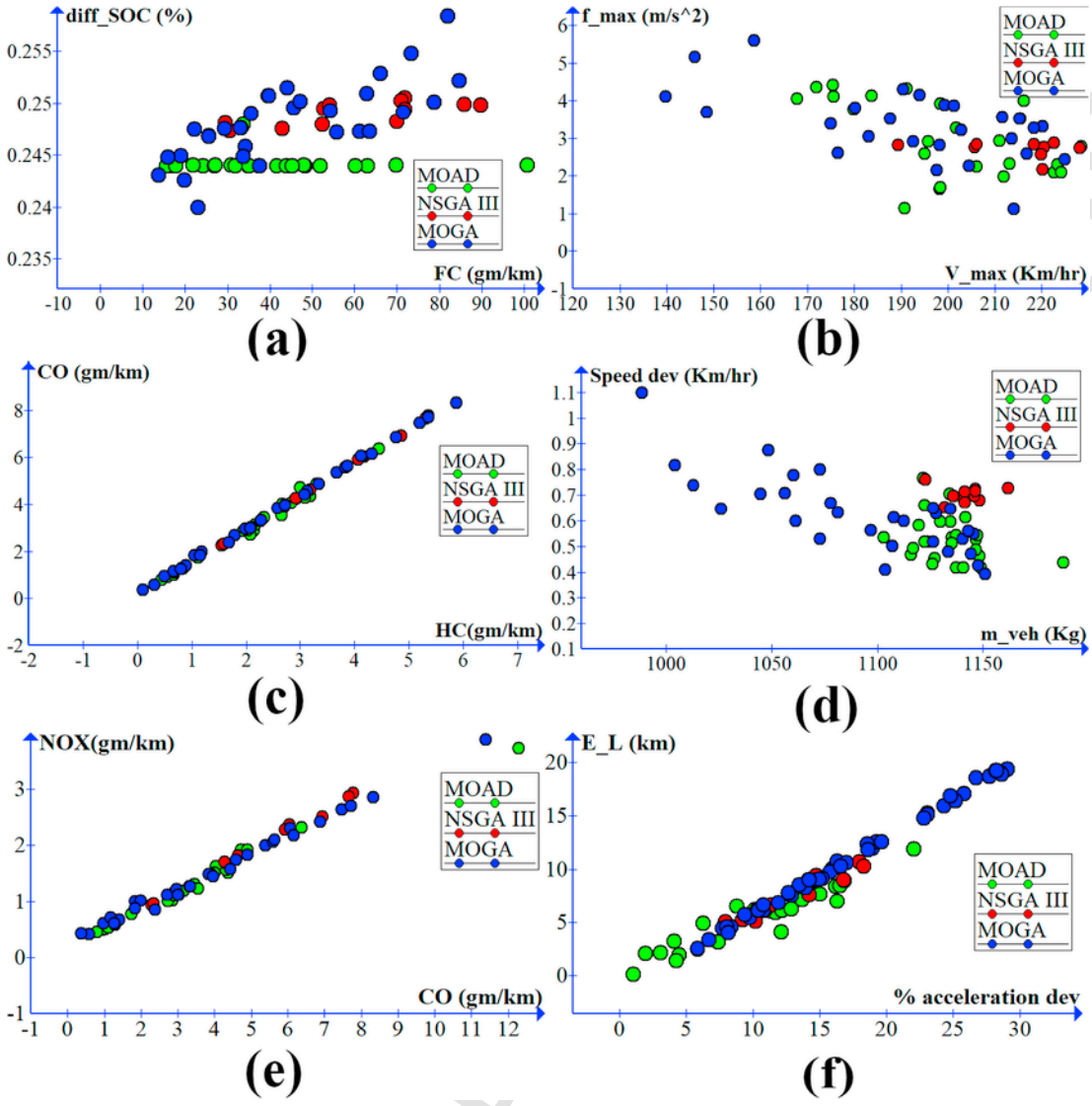

Fig. 12. 2D plots to show the correlations among objectives based on dominated solutions.

Table 7
Simulation results of 15 selected design points in FTP driving cycle.

#	P_{maxeng}	N_{bat}	P_{maxmot}	P_{maxgen}	N_r	N_s	i_0	m_{veh}	FC	Diff_SOC	HC	CO	NOX	V_{max}	f_{max}	OE_D	
1	48	50	32	12	58	32	2.741	1180	4.2	0.164	0.563	0.625	0.121	216.1	2.9	0.112	MOGA
2	28	43	50	30	58	26	3.999	1188	3.4	0.175	0.351	0.446	0.112	159.7	3.4	0.139	
3	46	50	38	9	64	26	2.776	1182	4.1	0.167	0.543	0.605	0.118	210.9	3.4	0.113	
4	46	32	27	22	59	19	3.653	1166	4.3	0.171	0.569	0.611	0.114	174.7	3.4	0.11	
5	49	50	35	9	57	29	2.169	1184	4.5	0.177	0.582	0.639	0.122	204.8	2.5	0.104	
6	47	18	40	8	57	39	3.91	1148	4.8	0.202	0.632	0.655	0.118	163.7	4.6	0.102	MOEA/D
7	48	30	41	6	58	36	3.977	1160	4.4	0.188	0.585	0.621	0.115	160.4	4.7	0.106	
8	43	16	45	6	60	35	3.865	1139	4.7	0.2064	0.579	0.608	0.116	166.3	4.7	0.102	
9	45	37	39	10	54	33	3.885	1169	4.1	0.1696	0.537	0.586	0.112	164.1	4.7	0.116	
10	41	21	43	7	55	35	3.975	1137	4.3	0.1961	0.541	0.595	0.118	161	4.7	0.114	
11	43	27	44	5	63	36	3.893	1148	4.3	0.1956	0.547	0.598	0.117	164.2	4.7	0.108	
12	47	21	38	6	52	32	3.501	1144	4.6	0.2012	0.566	0.563	0.103	183.7	4	0.099	
13	50	21	30	8	73	31	3.519	1139	4.6	0.1955	0.644	0.67	0.117	182.5	3.6	0.103	
14	48	29	35	9	54	27	3.052	1157	4.4	0.1833	0.609	0.65	0.119	192	3.6	0.108	NSGA III
15	48	13	33	6	89	26	3.473	1128	5.1	0.213	0.658	0.655	0.112	185.5	3.5	0.094	
CV	70	–	–	–	–	–	1	1195	7.4	–	0.429	1.494	0.24	211	4.1	0.069	BM[a]
TP	43	25	31	15	78	30	3.93	1404	4.9	0.1726	0.542	0.617	0.134	163	3.3	0.126	

[a] BM-Base Model.

Table 8
Validation results with respect to FTP driving cycle.

	SAEAs	m_{veh}	FC	Diff_SOC	HC	CO	NOX	V_{max}	f_{max}
Conventional Powertrain	MOGA	1.255%	46.47%	–	−21.585%	60.83%	51.08%	−8.42%	−23.90%
	MOEAD	3.933%	39.53%	–	−25.889%	59.04%	52.29%	−20.27%	8.84%
	NSGA III	4.393%	35.81%	–	−47.668%	56.33%	51.88%	−10.55%	−13.41%
Toyota Prius Powertrain	MOGA	15.954%	16.32%	1.04%	3.764%	6.67%	12.39%	18.55%	−5.45%
	MOEAD	18.234%	8.67%	−12.57%	−6.803%	0.81%	14.55%	3.21%	35.23%
	NSGA III	18.625%	3.06%	−14.83%	−16.881%	−5.754%	13.81%	15.79%	−7.58%

'+' indicates gain; '-' indicates loss.

2.1.5. Transmission modeling

Eq. (24)-(26) demonstrate the vehicle transmission model. The angular velocity and torque distributions are portrayed in Eq. (24) and Eq. (25) respectively.

$$\omega_{out} = \frac{1+k}{k}\omega_{eng} - \frac{1}{k}\omega_{mot} \tag{24}$$

$$\tau_{out} = \tau_{eng}\frac{k}{1+k} + \tau_{gen} \tag{25}$$

where k is the ratio of the N_r and sun gear N_s,

$$k = \frac{N_r}{N_s} \tag{26}$$

2.1.6. Vehicle dynamics

Based on these components of powertrain the vehicle dynamics can be represented using Eq. (27) [26].

$$\tau_w = \eta_g \eta_0 i_g i_0 \left(\tau_{eng} + \tau_{mot} + \tau_{gen}\right) + \tau_b \tag{27}$$

The acceleration is expressed using Eq. (28).

$$a = \frac{1}{\delta m_{veh}}\left(\frac{\tau_w}{r_w} - m_{veh} g f_r cos\theta - \frac{1}{2} C_D A \rho_{air} v_{veh}^2 - m_{veh} g sin\theta\right) \tag{28}$$

The battery power is expressed as P_{bat} in Eq. (29).

$$P_{bat} = \tau_{mot}\omega_{mot}\mu_{mot} + \frac{\tau_{gen}\omega_{gen}}{\mu_{gen}} \tag{29}$$

The overall efficiency of the powertrain could be defined using Eq. (30).

$$\mu_{veh} = \frac{m_{veh}\, v_{veh} g f_r cos\theta + \frac{1}{2} C_D A \rho_{air} v_{veh}^3}{P_{eng} + P_{bat}} \tag{30}$$

The percentage grade could be defined using Eq. (31),

$$\%Grade = 100 \times tan\theta \tag{31}$$

Interested readers could also consult ref. [27] for more details of powertrain components modeling.

2.1.7. PMS

The component sizing phenomenon and power management strategy are mutually related. The PMS strategies of ref. [28] is adopted in this study, which is elaborated in Table 2.

3. Research methodology

HEV powertrain optimization problem considered as one of the popular problems in non-conventional vehicle research. In this paper, NSGA III and MOEA/D are implemented with surrogate fitness function based on the BNN. To improve solution variations, regression assisted MOGA is used. The proposed methods are not compared mutually, but all the Pareto solutions are combined, which defines the feasible region of the best design points.

3.1. Surrogate assisted optimization

The SAEA is one of the latest trends being followed in Evolutionary Computing research, which is useful for computationally expensive problems. The ANN, DT, GP, SVM, etc. are popular as surrogates fitness functions [29]. When SAEA is implemented for multi-objective hybrid powertrain, the best practice is to utilize the data-driven functional approximation for fitness evaluation. SAEA often facilitates the use of the existing optimization algorithms, such as, EA, GA, DE, GP, etc. SAEA is capable of approximating functional relationships among process parameters based on sampled data obtained using DOE techniques [30]. Once the surrogate model is trained, an appropriate EA could be employed to find the optimal set of parameters [31]. Data-driven SAEA is substantially prompt and efficient; therefore, this is computationally inexpensive. DOE based tools, such as the LHS, FFD, and OAD etc. are generally used to define the experimental plan as initial population and input data to the surrogate models. SAEAs are being practiced in various engineering and technological research currently. Ref. [32] developed a two stage surrogate-assisted PSO algorithm by incorporating a global and some local surrogate functions. The proposed technique is tested with some popular unimodal and multimodal problems. Ref. [33] demonstrated online and off-line based classification of the surrogate assisted optimization techniques and developed an EA to optimize the offline data-driven trauma system. Ref. [34] performed a survey based on a surrogate based global optimization. Authors put focus on the balance between exploration and exploitation search. Gaussian Process or Kriging based surrogate models are reviewed primarily. Ref. [35] studied combined effect of surrogate-assisted PSO and a surrogate-assisted social learning algorithm, which worked on exploration and PSO worked on exploitation and tested on benchmark problems. Ref. [36] discussed five real-world cases of Blast Furnace Optimization, Trauma System Design Optimization, Optimization of Fused Magne-

sium Furnaces, Optimization of Airfoil Design, and Air Intake Ventilation System where SAEAs have shown promising solutions.

The hybrid powertrain optimization problem could be categorised as a many-objective optimization problem. The problem dimension is complex as 7 decision variables and 11 objectives are considered. This article attempts to solve such a complex problem, which is not yet available in literature. The main objectives are to improve the performances, emissions and fuel consumptions of the HEV. Fuel consumption is defined using FC and diff_SOC. The emission expressions are derived from HC, CO, NOX. The other performance indicators are considered as m_{veh}, % acceleration dev, E_L, speed dev, V_max, and f_-max. These accomplish the 11 objectives. The decision variables considered are P_{maxeng}, P_{maxmot}, N_{bat}, P_{maxgen}, N_r, N_s, and i_0. The major constraints of the problem are used as the viable ranges for each of the variables and the vehicle weights (pre-defined upper bound).

3.2. SAEAs

In this work, NSGA III and MOEA/D assisted by BNN, and Regression model assisted MOGA are used as SAEAs.

3.2.1. BNN

BNN is conceptualized on Bayes' rule, which considers the relationship between the probability of any process and prior knowledge of it. The output responses (posterior) are generated using this relationship. Ref. [37] has expressed the probability density function of weights as,

$$P(w|d,\alpha,\ \beta,\ M) = \frac{P(D|w,\ \beta,M)\,P(w|\alpha,M)}{P(D|\alpha,\beta,M)} \tag{32}$$

where D is data, M is the type of neural network (Multi-Layer Perceptron), w is the vector of network weights. P(w|α, M) denotes prior knowledge of the weights. P(D|w, β, M) is likelihood and P(D|α, β, M) is normalization factor. When noise in D and P(w|α, M) are Gaussian, then likelihood and normalization factor are expressed as,

$$P(D|w,\ \beta,M) = \frac{1}{Z_D(\beta)}e^{-\beta E_D} \tag{33}$$

$$P(w|\alpha,M) = \frac{1}{Z_w(\alpha)}e^{-\alpha E_w} \tag{34}$$

where $Z_D(\beta) = (\pi/\beta)^{n/2}$ *and* $Z_w(\beta\alpha) = (\pi/\alpha)^{N/2}$. E_D is the sum of squared errors for data and E_W is the sum of squares for weights. Hence, Eq. (32) becomes,

$$P(w|d,\alpha,\ \beta,\ M) = \frac{\frac{1}{Z_D(\beta)Z_w(\alpha)}e^{-(\beta E_D+\alpha E_w)}}{P(D|\alpha,\beta,M)} \tag{35}$$

$$= \frac{1}{Z_F(\alpha,\beta)}e^{-(\beta E_D+\alpha E_w)} \tag{36}$$

Optimal weights maximize the posterior probability density function P(w|D, α, β, M), which is equivalent to minimization of regularized objective function $f = (\beta.E_D+\alpha.E_w)$. α and β are governed by Bayesian Regularization. BNN is a probabilistic network. The input variables are generally treated as probability density function to the hidden layer [38]. The output obtained is spanned over a new distribution, which improves the prediction accuracy. Fig. 5 shows the BNN schematic.

3.2.2. MOEA/D

MOEA/D [39] is initially developed for multi-objective optimization problems, which decomposes the main problem into small sub-problems. In the MOEA/D optimization process, the neighbourhood relationships among the objectives are used in genetic operation. The MOEA/D could be fused with other methods for its general framework. The different hybrid model of MOEA/D can be found in the articles [40,41]. The flowchart of MOEA/D is presented in Fig. 6(a).

3.2.3. NSGA III

NSGA III is an improved version of NSGA II for many-objective optimization, which is proposed recently [42]. Unlike NSGA II, a number of reference points with good distribution are employed to guide the selection of non-dominated solutions for next generation instead of using crowding distance for diversity control in NSGA III. In fact, the use of multiple reference points in NSGA III plays an important role for guiding the population to converge towards the Pareto front along different search directions. Over the past couple of years, NSGA III has become the baseline multi-objective EA for performance measurement for many-objective optimization. The basic NSGA III algorithm is depicted in Fig. 6(b).

3.2.4. MOGA

MOGA is a heavily explored method for solving the MOPs [43–45]. MOPs are popularly solved using weighted sum approach. MOGA follows the simple GA structure with all the genetic operators, namely selection, crossover, and mutation. The MOGA flowchart has been provided in Fig. 7.

3.2.5. Regression models

For the MOGA, regression models for the HEV powertrain optimization are used as fitness functions, which are developed for all the 11 objectives at 95% confidence level considering seven input parameters. Eq. (37) to Eq. (47) portray the regression models.

$$\begin{aligned} m_{veh} = {} & 881.167 + 2.8 \times P_{maxeng} + 1.9 \times P_{maxmot} \\ & + 2.2 \times P_{maxgen} + 1.15 \times N_{bat} \end{aligned} \tag{37}$$

$$\begin{aligned} FC = {} & 166.7 - 1.026 \times P_{maxeng} - 0.09 \times P_{maxmot} \\ & + 0.504 \times P_{maxgen} - 28.11 \times i_0 - 1.037 \\ & \times N_{bat} + 0.760 \times N_r - 0.644 \times N_s \end{aligned} \tag{38}$$

$$\begin{aligned} \%\text{accelearation dev} = {} & 45.04 - 0.2905 \times P_{maxeng} \\ & - 0.0387 \times P_{maxmot} - 0.0684 \\ & \times P_{maxgen} - 4.727 \times i_0 \\ & - 0.0631 \times N_{bat} + 0.1026 \\ & \times N_r - 0.3594 \times N_s \end{aligned} \tag{39}$$

$$\begin{aligned} HC = {} & 11.36 - 0.0568 \times P_{maxeng} - 0.0066 \times P_{maxmot} \\ & + 0.0359 \times P_{maxgen} - 1.954 \times i_0 - 0.0817 \\ & \times N_{bat} + 0.0672 \times N_r - 0.1029 \times N_s \end{aligned} \tag{40}$$

$$CO = 16.13 - 0.0874 \times P_{maxeng} - 0.0092 \times P_{maxmot} + 0.0516 \times P_{maxgen} - 2.773 \times i_0 - 0.1117 \times N_{bat} + 0.0932 \times N_r - 0.1318 \times N_s \quad (41)$$

$$NOX = 5.43 - 0.0327 \times P_{maxeng} - 0.0024 \times P_{maxmot} + 0.019 \times P_{maxgen} - 0.947 \times i_0 - 0.0354 \times N_{bat} + 0.02848 \times N_r - 0.0277 \times N_s \quad (42)$$

$$E_L = 32.75 - 0.1944 \times P_{maxeng} - 0.0411 \times P_{maxmot} - 0.0778 \times P_{maxgen} - 3.196 \times i_0 - 0.0583 \times N_{bat} + 0.0488 \times N_r - 0.2519 \times N_s \quad (43)$$

$$\text{Speed dev} = 1.626 - 0.00535 \times P_{maxeng} - 0.00286 \times P_{maxmot} - 0.00334 \times P_{maxgen} - 0.1211 \times i_0 - 0.00506 \times N_{bat} + 0.00164 \times N_r - 0.00857 \times N_s \quad (44)$$

$$diff_{SOC} = 0.28169 - 0.000209 \times P_{maxeng} - 0.000058 \times P_{maxmot} - 0.000261 \times P_{maxgen} - 0.002719 \times i_0 - 0.000079 \times N_{bat} + 0.000027 \times N_r - 0.000385 \times N_s \quad (45)$$

$$V_{max} = 252.9 + 0.144 \times P_{maxeng} - 0.098 \times P_{maxmot} - 0.807 \times P_{maxgen} - 26.27 \times i_0 + 0.802 \times N_{bat} + 0.273 \times N_r - 0.556 \times N_s \quad (46)$$

$$f_{max} = -1.485 - 0.00722 \times P_{maxeng} + 0.06389 \times P_{maxmot} + 0.02 \times P_{maxgen} + 0.842 \times i_0 + 0.01111 \times N_{bat} - 0.00754 \times N_r + 0.0037 \times N_s \quad (47)$$

The model competencies are determined using the determination coefficients (R^2) values. Higher the R^2 values, better is the model fitting (Table 3). For NSGA III and MOEA/D, the BNN surrogate (in #3.2.1) is opted as the fitness function. The basic SAEA framework is portrayed in Fig. 8, which is the generalized form of SAEAs for HEV powertrain optimization.

4. Results and discussions

The initial modeling data for powertrain are generated with ADVISOR software of NREL [27] and MATLAB. The proposed SAEAs are also developed in MATLAB on an Intel i7 8650U Laptop. Taguchi's OAD is employed to present the experimental plan, where the levels of each factor are defined with three levels (Table 4) and L^{27} table is shown in Table 5 with the input variables and target responses.

It is important to initialize the BNN before training. Incorrect initialization could lead to the premature convergence. It also affect the convergence speed or computing time. BNN parameters are set as, learning rate = 0.01, error goal = 1e-10, and number of epochs = 3500. Data from Table 5 are used as the training and validation data (70:30). The cross validation is not considered since very low MSE value is obtained during the training and accurate responses are predicted. The BNN stops when the MSE score converges or the maximum number of epochs is reached. The BNN stops at 2492nd epoch with very low MSE value of 2.8701e-06 since there is no further improvement noticed. The performance of the BNN surrogate could be observed in Figs. 9 and 10. It could be observed from Fig. 9 that the BNN training yields high accuracy with low MSE score. That is further validated using Fig. 10, which demonstrates accurate data fitting for all the responses. For all the SAEAs, parameters are set as, Maximum number of generations = 500, Population Size = 200; Crossing over probability = 0.6, and Mutation rate = 0.05.

The initial results for all the SAEA methods are depicted as the probability distributions for all the eleven objectives in Fig. 11(a)–(c). A summary of the comparison study is portrayed in Table 6. It could be observed that NSGA III produces better results for major number of objectives, such as FC, % accelearation_dev, HC, CO, NOX, Failed to travel distance, V_{max} and f_{max}. In case of speed deviation and $diff_{SOC}$, MOEA/D produces better results; on the other hand, MOGA reduces the vehicle weight significantly. Out of the 475 solution samples, only 78 feasible solutions are selected based on (a) the peak power of the generator, which is believed to be less than the primary motor and (b) the speed deviation, which should be within the length of the driving cycle for 20% road grade. Fig. 11(d) shows the 78 design points as probability density distribution and the average downsizing of engine from 70 kW to 41.94 kW which is approximately 42 kW. So 40.1% or 40% approximate downsizing can be achieved.

Whereas, Fig. 12 depicts the objective trade-offs in duos for the 78 design points. Not every combination of objectives are pertinent to this study (e.g. emissions vs. weight, fuel efficiency vs. emission, fuel efficiency vs. torque or acceleration etc.). Most relevant objective combinations are displayed such as the fuel efficiencies, emissions, acceleration vs. torque, speed vs. vehicle weight, and acceleration error vs. distance failed to travel. Fig. 12(a) considers two types of fuel consumptions, SOC change vs. fossil fuel usage. It could be observed that the MOEA/D results do not change with consumed SOC but change uniformly with fossil fuel consumption, and the MOGA and NSGA III results are distributed evenly in for both the objectives. Fig. 12(b) and (c) show the trade-offs among emission related objectives, which are correlated and proportional in nature. Fig. 12(d) presents the relationships between the maximum speed and maximum acceleration. It could be noted that maximum acceleration produces low velocity; whereas maximum velocity could be reached with medium acceleration. The other two objectives, vehicle weight and speed error are portrayed in Fig. 12(e), which confirms that the extreme reduction in weight could produce higher speed errors. Finally, the distance failed to travel and percentage acceleration deviation are shown in Fig. 12(f), which are proportionally correlated.

4.1. Validation test

Total 15 solution points (Table 7) are selected for validation test through the simulation and the different responses are recorded. Percent acceleration deviation, speed error and failed to travel distance are excluded as these responses obtain zero values. OE_D has been incorporated to show further efficiency improvements. Based on the measured responses and predicted responses, the summary of the improvements is presented in the Table 8, which presents eight objectives (excluding percent acceleration deviation, speed error and failed to travel distance). It could be noted that the top 15 selected feasible solutions consist of 5, 8, and 2 solutions obtained by MOGA, MOEA/D, and NSGA III respectively. The NSGA III and MOEA/D

downgrade the average weight of vehicle by 4.39%, 3.93% respectively.

MOGA and MOEA/D reduce the fuel consumption by 46.47% and 39.53% respectively. On the other hand, the CO emission is 60.83% reduced by MOGA. In case of NOX emission, the MOEA/D produces better solutions by 52.29%. In case of maximum velocity, the MOGA obtains inferior solution by at least 8.42% and MOEA/D gains acceleration by 8.84%. In case of HC and maximum speed, none of the SAEAs shows improvement. While comparing with Toyota Prius model, maximum weight reduction is achieved the NSGA III. For fossil fuel consumption, MOGA produces 16.32% improvement. In case of SOC change, MOGA produces improvement of 1.04%. MOGA produces better result for HC and CO emission. For NOX, MOEA/D produces better result. In case of maximum speed, MOGA and NSGA III produce improvement of 18.55% and 15.79% respectively. In case of acceleration, MOEA/D produces enhancement of 35.23%. For energy efficiency, the MOGA produces better energy efficient powertrains. In case of 15 selected points, MOGA produces better results in FTP driving cycle but NSGA III produces improved results for UDDS driving cycle. The overall average powertrain efficiency has been improved by 57.49%.

5. Conclusion

In this study, an effort is made to solve the many-objective hybrid powertrain model, which considered 7 decision variables and 11 responses. The problem model is substantially complex and computationally expensive. Initially, the simulation model is utilized to obtain the responses. Thereafter state-of-the-art SAEAs are introduced based on NSGA III, MOEA/D and MOGA. BNN and regression models are used as surrogates. The proposed SAEAs are shown to obtain interesting results. Following conclusions are drawn from this study.

- Considering a large number of objectives could improve the responses for HEV powertrain optimization. This approach obtains a lighter vehicle with reduced weight and engine size by 4.39% and 40.1% respectively.
- The overall energy efficiency is improved for the solutions while compared with the conventional vehicle model.
- Since the global optimal solutions are not guaranteed by heuristic SAEAs, the Pareto fronts define the best feasible design points in the bounded design space.
- Design points are obtained for the UDDS driving cycle for 20% grade; therefore, the solutions are more efficient in the higher grade and the average engine size is more than the motor size.
- In overall analysis for UDDS driving cycle, the NSGA III portrays improvements for most of the objectives and MOGA and MOEA/D both produce competitive results for FTP driving cycle.

This work could be extended further to obtain (1) the global best solutions for HEV powertrain optimization and (2) Finite Element Method model for power-split device to improve the fuel consumptions and performances further.

References

[1] B. Caulfield, S. Farrell, B. McMahon, Examining individuals preferences for hybrid electric and alternatively fuelled vehicles, Transport Pol 17 (6) (2010) 381–387.

[2] Y. Huang, H. Wang, A. Khajepour, B. Li, J. Ji, K. Zhao, C. Hu, A review of power management strategies and component sizing methods for hybrid vehicles, Renew Sustain Energy Rev 96 (2018) 132–144.

[3] L. Xu, C.D. Mueller, J. Li, M. Ouyang, Z. Hu, Multi-objective component sizing based on optimal energy management strategy of fuel cell electric vehicles, Appl Energy 157 (2015) 664–674.

[4] V. Herrera, A. Milo, H. Gaztañaga, I. Etxeberria-Otadui, I. Villarreal, H. Camblong, Adaptive energy management strategy and optimal sizing applied on a battery-supercapacitor based tramway, Appl Energy 169 (2016) 831–845.

[5] N. Murgovski, S. Marinkov, D. Hilgersom, B. d. Jager, M. Steinbuch, J. Sjöberg, Powertrain sizing of electrically supercharged internal combustion engine vehicles, In: IFAC-PapersOnLine, 2015.

[6] Y.-H. Hung, C.-H. Wu, A combined optimal sizing and energy management approach for hybrid in-wheel motors of EVs, Appl Energy 139 (2015) 260–271.

[7] N.L. Azad, A. Mozaffari, M. Vajedi, Y. Masoudi, "Chaos oscillator differential search combined with Pontryagin's minimum principle for simultaneous power management and component sizing of PHEVs, Optim Eng 17 (4) (2016) 727–760.

[8] Z. Song, J. Hou, S. Xu, M. Ouyang, J. Li, The influence of driving cycle characteristics on the integrated optimization of hybrid energy storage system for electric city buses, Energy 135 (2017) 91–100.

[9] H.K. Roy, A. McGordon, P.A. Jennings, A generalized powertrain design optimization methodology to reduce fuel economy variability in hybrid electric vehicles, IEEE Trans Veh Technol 63 (3) (2014) 1055–1070.

[10] O.H. Dagci, O.H. Dagci, H. Peng, J.W. Grizzle, Hybrid electric powertrain design methodology with planetary gear sets for performance and fuel economy, IEEE Access 6 (2018) 9585–9602.

[11] Q. Zhou, W. Zhang, S. Cash, O. Olatunbosun, H. Xu, G. Lu, Intelligent sizing of a series hybrid electric power-train system based on Chaos-enhanced accelerated particle swarm optimization, Appl Energy 189 (2017) 588–601.

[12] X. Zhou, D. Qin, J. Hu, Multi-objective optimization design and performance evaluation for plug-in hybrid electric vehicle powertrains, Appl Energy 208 (2017) 1608–1625.

[13] A.P. Vora, X. Jin, V. Hoshing, T. Saha, G. Shaver, S. Varigonda, O. Wasynczuk, W.E. Tyner, Design-space exploration of series plug-in hybrid electric vehicles for medium-duty truck applications in a total cost-of-ownership framework, Appl Energy 202 (2017) 662–672.

[14] D. Jung, Q. Ahmed, G. Rizzoni, Design space exploration for powertrain electrification using Gaussian processes, In: Annual American control conference, ACC, 2018.

[15] F. Millo, C. Cubito, L. Rolando, E. Pautasso, E. Servetto, Design and development of an hybrid light commercial vehicle, Energy 136 (2017) 90–99.

[16] S. Geng, A. Meier, T. Schulte, Model-based optimization of a plug-in hybrid electric powertrain with multimode transmission, World Electric Vehicle Journal 9 (1) (2018) 12.

[17] J. Kim, G. Kim, Y. -i. Park, Component sizing of parallel hybrid electric vehicle using optimal search algorithm, Int J Automot Technol 19 (4) (2018) 743–749.

[18] Z. Qin, Y. Luo, K. Li, H. Peng, Optimal design of single-mode power-split hybrid tracked vehicles, ournal of Dynamic Systems, Measurement, and Control 140 (10) (2018) 101002.

[19] M. Pourabdollah, B. Egardt, N. Murgovski, A. Grauers, Convex optimization methods for powertrain sizing of electrified vehicles by using different levels of modeling details, IEEE Trans Veh Technol 67 (3) (2018) 1881–1893.

[20] C. Angerer, M. Felgenhauer, I. Eroglu, M. Zähringer, S. Kalt, M. Lienkamp, Scalable dimension-, weight-and cost-modeling for components of electric vehicle powertrains, In: 2018 21st international conference on electrical machines and systems, ICEMS, 2018.

[21] S. Cash, Q. Zhou, O. Olatunbosun, H. Xu, S. Davis, R. Shaw, New traction motor sizing strategy for an HEV/EV based on an overcurrent-tolerant prediction model, IET Intell Transp Syst 13 (1) (2018) 168–174.

[22] Z. Song, X. Zhang, J. Li, H. Hofmann, M. Ouyang, J. Du, Component sizing optimization of plug-in hybrid electric vehicles with the hybrid energy storage system, Energy 144 (2018) 393–403.

[23] H. Guo, Q. Sun, C. Wang, Q. Wang, S. Lu, A systematic design and optimization method of transmission system and power management for a plug-in hybrid electric vehicle, Energy 148 (2018) 1006–1017.

[24] Y. Yang, H. Pei, X. Hu, Y. Liu, C. Hou, D. Cao, Fuel economy optimization of power split hybrid vehicles: a rapid dynamic programming approach, Energy 166 (2019) 929–938.

[25] F. Lei, Y. Bai, W. Zhu, J. Liu, A novel approach for electric powertrain optimization considering vehicle power performance, energy consumption and ride comfort, Energy 167 (2019) 1040–1050.

[26] Y. Wang, X. Wang, Y. Sun, S. You, Model predictive control strategy for energy optimization of series-parallel hybrid electric vehicle, J Clean Prod 199 (2018) 348–359.

[27] A. Brooker, K. Haraldsson, T. Hendricks, V. Johnson, K. Kelly, B. Kramer, T. Markel, M. O'Keefe, S. Sprik, K. Wipke, ADVISOR advanced vehicle simulator, [Online]. Available: http://adv-vehicle-sim.sourceforge.net/, 26 March 2013Accessed 3 March 2019.

[28] D. Bhattacharjee, P. Bhola, P.K. Dan, Fuzzy based propulsion selection for fuel efficiency in hybrid electric vehicle, In: ASME 2018 international design engineering technical conferences and computers and information in engineering conference, Canada, Quebec, 2018.

[29] C. Gröger, F. Niedermann, B. Mitschang, Data mining-driven manufacturing process optimization, London, 2012.
[30] Y. An, W. Lu, W. Cheng, "Surrogate model application to the identification of optimal groundwater exploitation scheme based on regression kriging method—a case study of western jilin province, Int J Environ Res Public Health 12 (8) (2015) 8897–8918.
[31] A. Messac, Optimization in practice with MATLAB, Cambridge University Press, NY, USA, 2015.
[32] C. Sun, Y. Jin, J. Zeng, Y. Yu, A two-layer surrogate-assisted particle swarm optimization algorithm, Soft Computing 19 (6) (2015) 1461–1475.
[33] H. Wang, Y. Jin, J.O. Jansen, Data-driven surrogate-assisted multiobjective evolutionary optimization of a trauma system, IEEE Trans Evol Comput 20 (6) (2016) 939–952.
[34] R.T. Haftka, D. Villanuev, A. Chaudhuri, "Parallel surrogate-assisted global optimization with expensive functions – a survey, Struct Multidiscip Optim 54 (1) (2016) 3–13.
[35] C. Sun, Y. Jin, R. Cheng, J. Ding, J. Zeng, Surrogate-assisted cooperative swarm optimization of high-dimensional expensive problems, IEEE Trans Evol Comput 21 (4) (2017) 644–660.
[36] Y. Jin, H. Wang, T. Chugh, D. Guo, K. Miettinen, Data-driven evolutionary optimization: an overview and case studies, IEEE Trans Evol Comput (2018).
[37] F.D. Foresee, M.T. Hagan, Gauss-Newton approximation to Bayesian learning, In: Proceedings of international conference on neural networks, ICNN'97, Houston, TX, USA, USA, 1997.
[38] J.T. Springenberg, A. Klein, S. Falkner, F. Hutter, Bayesian optimization with robust bayesian neural networks, In: Neural information processing systems, NIPS, 2016.
[39] Q. Zhang, H. Li, MOEA/D: a multiobjective evolutionary algorithm based on decomposition, IEEE Trans Evol Comput 11 (6) (2007) 712–731.
[40] Z. Wang, Q. Zhang, A. Zhou, M. Gong, L. Jiao, Adaptive replacement strategies for MOEA/D, IEEE Transactions on Cybernetics 46 (2) (2016) 474–486.
[41] H. Sato, Inverted PBI in MOEA/D and its impact on the search performance on multi and many-objective optimization, In: Proceedings of the 2014 annual conference on genetic and evolutionary computation, Canada, Vancouver, BC, 2014.
[42] H. Jain, K. Deb, An evolutionary many-objective optimization algorithm using reference-point-based nondominated sorting approach, Part II: handling constraints and extending to an adaptive approach, IEEE Trans Evol Comput 18 (4) (2014) 602–622.
[43] C.M. Fonseca, P.J. Fleming, Genetic algorithms for multiobjective optimization: FormulationDiscussion and generalization, In: Proceedings of the 5th international conference on genetic algorithms, 1993.
[44] Y. Ge, S. Wang, Z. Liu, W. Liu, Optimal shape design of a minichannel heat sink applying multi-objective optimization algorithm and three-dimensional numerical method, Appl Therm Eng 148 (2019) 120–128.
[45] H. Sun, Y. Gea, W. Liu, Z. Liu, Geometric optimization of two-stage thermoelectric generator using genetic algorithms and thermodynamic analysis, Energy 171 (2019) 37–48.